Catalysis Today 143 (2009) 69–75

Contents lists available at ScienceDirect

Catalysis Today

journal homepage: www.elsevier.com/locate/cattod

Identification of Ru phases in PtRu based electrocatalysts and relevance in the methanol electrooxidation reaction

J.L.Gómez de la Fuente [a,*], F.J. Pérez-Alonso [b], M.V. Martínez-Huerta [b], M.A. Peña [b], J.L.G. Fierro [b], S. Rojas [b]

[a] Department of Materials Science and Engineering, Norges Teknisk-Naturvitenskapelige Universitet (NTNU), C/Sem Sælandsvei 12, NO-7491 Trondheim, Norway
[b] Instituto de Catálisis y Petroleoquímica, CSIC, C/Marie Curie 2, 28049 Madrid, Spain

ARTICLE INFO

Article history:
Available online 25 March 2009

Keywords:
Electrocatalyst
Methanol
PtRu
Amorphous ruthenium oxide
XPS

ABSTRACT

A relationship between the chemical state of Ru on bimetallic PtRu bulk samples and their performance in both CO and methanol electrooxidation has been established. The nature of the Ru species in the bimetallic samples has been scrutinized by means of XPS, XRD and TPR. The following Ru species were detected; reduced ruthenium (Ru^0), anhydrous RuO_2 and hydrous Ru oxide. The actual nature of the latter species consists of two amorphous oxides of general formula $RuO_2{\cdot}xH_2O$ and $RuO_x(OH)_y$ as determined from the XPS analysis. Irrespective of the Ru phases, all PtRu catalyst studied display a similar CO oxidation pattern. However, methanol electrooxidation was found dependent on the Ru phases. Thus, catalysts containing Ru^0 are more active in the methanol oxidation reaction, at least during the early stages of the reaction. More stable catalyst are obtained if amorphous Ru oxide phases are the predominant ones.

1. Introduction

Bimetallic surfaces have been known for their especial catalytic properties, which often exceed those of their individual components. This is particularly important for the development of highly active and stable catalysts for electrocatalytic reactions such as methanol or CO electrooxidation and oxygen reduction reaction which are core processes of the so called direct methanol fuel cells (DMFCs). Platinum ruthenium bimetallic catalysts show superior performance (either in terms of activity or stability) than Pt alone in both CO and methanol electrooxidation reactions. Therefore PtRu catalysts are benchmark catalysts for DMFCs. Although still under debate, the bifunctional mechanism in which Ru provides OH_{ad} species at less positive potentials than Pt [1] is the most accepted. The role of Ru in weakening the strength of the CO bond to Pt (ligand effect) cannot be neglected either [2].

$RuO_x(OH)_y$ is a well known Ru species since is the active component in the chloralkali industry and an excellent energy storage material for supercapacitor applications [3]. This species conducts both electrons and protons and it has a high affinity for oxygen nucleation as OH at potentials below 0.4 V. These properties endow this Ru species with very interesting properties as electrocatalysts for CO and methanol electrooxidation [4,5].

It has been recognized that PtRu black are not single-phase materials, but bulk mixtures of Pt metal, Pt hydrous oxides and hydrous and dehydrated RuO_2 [6]. In the same line, hydrous ruthenium oxide has been reported to be a mixture of non-stoichiometric oxoruthenium states, involving at least three oxygen-containing species and H_2O. In fact, H_2O is the source of both oxygen and hydroxyl groups [7,8].

The archetypal composition of the anodic electrocatalysts for DMFC consists of carbon supported PtRu nanoparticles. However, whether a real PtRu alloy is formed or not, and what is the oxidation state of their components, especially that of Ru is still under debate. To this end, X-ray photoelectron spectroscopy (XPS) technique is a powerful tool since it could disclose the actual oxidation state species on the catalyst surface. Unfortunately, the binding energy of C 1s core-level falls in the same energy region of Ru 3d levels (the principal photoelectronic contribution to the XPS spectrum of Ru). This feature may account to the lack of reliable references of the photoelectron binding energy for ruthenium compounds in electrocatalysts for DMFCs.

In this work, a comprehensive XPS study with special attention to the oxidation state of Ru is given. The aim of this study is to identify the most active Ru species during the electrooxidation reaction. It must be recalled that the XPS study has been undertaken on fresh samples.

* Corresponding author. Tel.: +47 735 94 127.
E-mail addresses: gomez@nt.ntnu.no, gofuen@gmail.com (J.L.Gómez de la Fuente).

0920-5861/$ – see front matter © 2008 Elsevier B.V. All rights reserved.
doi:10.1016/j.cattod.2008.10.052

2. Experimental

$RuCl_3$ and H_2PtCl_6 were supplied by Johnson Matthey. Fresh samples, denoted as Ru-fresh and PtRu-fresh (atomic ratio 1:1), were obtained by alkali precipitation with NaOH [9], samples were thoroughly washed to remove chlorine ions and dried at 100 °C for 4 h. Aliquots of fresh samples were subjected to reducing treatment under 10% H_2/Ar to a final temperature of 250 °C. The catalysts were labeled as Ru-reduced and PtRu-reduced. A further aliquot of PtRu-fresh was annealed under He atmosphere at 250 °C, sample labeled as PtRu-He. Ru-calcined was prepared by thermal treatment under O_2 at 800 °C of 10% Ru/C (obtained by impregnation of $RuCl_3$ on Vulcan XC 72R). Pt-reduced was obtained by reducing H_2PtCl_6 with $NaBH_4$, the solid was rinsed and dried at 100 °C during 4 h. RuAu-fresh was prepared by alkali precipitation [9], a fraction was treated in 10% H_2/Ar (RuAu-reduced). These samples were employed as internal references for the XPS analysis.

X-ray diffraction patterns were recorded using Cu Kα radiation in a Seiffert 3000 XPert X-ray diffractometer. Diffractograms were recorded between 15° and 90°. PowderCell software was used for data analysis [10]. Temperature programmed reduction (TPR) measurements were recorded in a Micromeritics TPR/TPO 2900 apparatus provided with a thermal conductivity detector (TCD). Typically, 30 mg of powder sample was heated from room temperature to 300 °C at 10 °C/min under a flow of 10% H_2/Ar gas mixture. Previously the samples were dried 1 h at 110 °C in He flow. XPS spectra have been collected in a VG Escalab 200R spectrometer using a Mg Kα X-ray source with a power of 120 W. Curve fitting was performed by employing least-squares fitting program (*XPS peak* software). This program permits linear or Shirley backgrounds, a mixture of Gaussian and Lorentzian peak shapes, as well as constrains on peak position (binding energy) and peak width. Binding energies of RuAu samples were calibrated by setting Au^0 $4f_{7/2}$ at 84.0 eV. In order to deconvolute the Ru 3d core region of the rest of the samples, parameters such as FWMH (full width at middle height), peak position (binding energy), GL (Gaussian to Lorentzian ratio) were set equal as those resulting from the fitting of RuAu samples, a summary of the analysis parameters is given in Table 2. Peak intensity was set as the only free parameter. Once the fitted and experimental spectra display a reasonable level of coincide, fine fitting was achieved by adjusting the spectra one further time letting all parameters free.

Electrochemical measurements were carried out in a standard three electrodes electrochemical cell at room temperature performed with a PC controlled potentiostat/galvanostat (Autolab PGstat 302N). Although referred to the NHE, potentials were measured versus Ag/AgCl electrode. A Pt wire was used as the counter electrode. A glassy carbon electrode (GC) (6 mm diameter) was used as the working electrode. For the CO oxidation measurements (CO stripping analysis), 0.5 M $HClO_4$ solution was used as electrolyte. The solution was purged with Ar before every experiment. Samples were activated by potentials excursions from 0.0 to 0.8 V at 50 mV/s until the recorded voltammograms remaining unchanged. Then CO was adsorbed at 20 mV during 15 min under stirring. After CO removal (Ar purge during $>$ 30 min) the working electrode was subjected to cyclic voltammetry program at 10 mV/s; three consecutive cycles were recorded. As control, the profile of the voltammogram obtained after CO oxidation was compared to those previously recorded.

For the methanol oxidation experiments, 0.5 M H_2SO_4 was used as electrolyte. The solution was degassed and the electrode was activated by 10 consecutive scans between 0 and 0.8 V (20 mV/s). Voltammogram profiles remained unchanged during the experiment. Chronoamperometric tests were recorded by setting the working electrode at 500 mV during 5 min to obtain the background response. Then, methanol (to a final concentration 2 M) was added and chronoamperometry test (500 mV/30 min) was recorded at 25 °C. The obtained current was normalized to the active area of the electrode deduced from the stripping analysis.

3. Results and discussion

3.1. Physicochemical characterization

3.1.1. XRD analysis

X-ray diffraction patterns of Ru-reduced, Ru-calcined and Ru-fresh samples are depicted in Fig. 1a. The diffractograms of the PtRu-fresh, PtRu-He and PtRu-reduced are depicted in Fig. 1b. Diffraction patterns of Pt (JCPDS 04-0802), Ru (JCPDS 6-663), RuO_2 (JCPDS 73-1469) are included for comparison. The diffraction

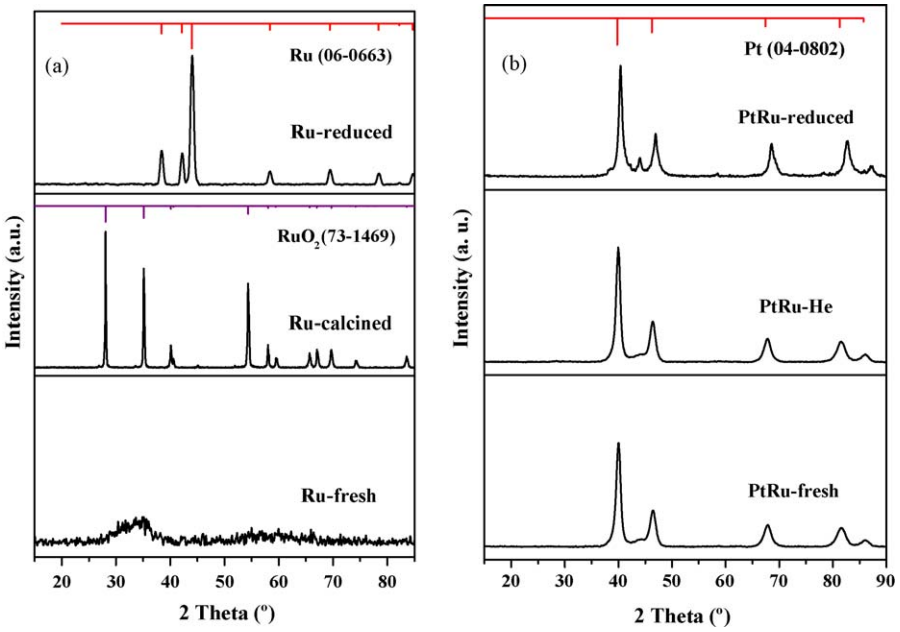

Fig. 1. Diffractograms of bare Ru samples (a) and PtRu (b). The diffraction lines of Ru (JCPDS 6-663), RuO_2 (JCPDS 73-1469) and Pt (04-0802) are included.

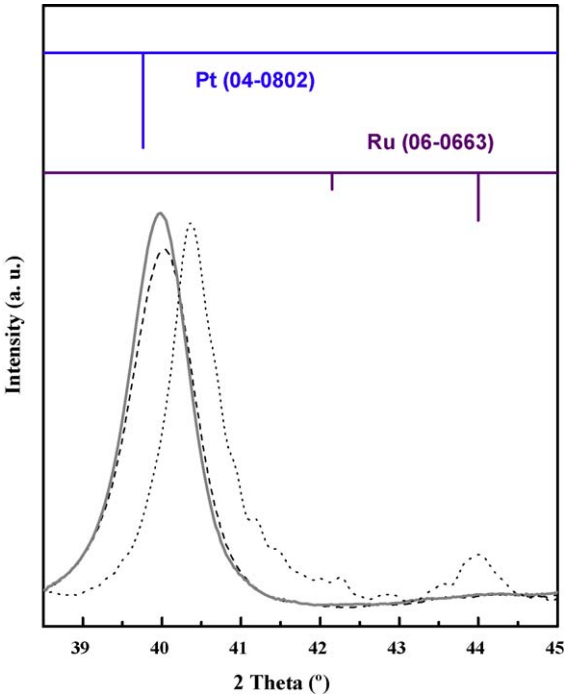

Fig. 2. Magnification of the diffractograms of PtRu-fresh (dash), PtRu-He (grey) and PtRu-reduced (dotted line).

patterns of Ru-reduced and Ru-calcined virtually coincide with those of Ru metallic (JCPDS 6-663) and RuO_2 (JCPDS 73-1469), respectively. On the other hand, Ru-fresh displays an ill defined diffractogram corresponding to an amorphous structure. The diffractogram of PtRu-fresh and PtRu-He samples display the characteristic peaks of a Pt fcc structure. A shifting of the Pt fcc reflections to higher 2θ is observed after subjecting the sample to a reducing atmosphere, *i.e.* sample PtRu-reduced. The magnitude of the shifting is clearly observed in Fig. 2. This shifting has been often attributed to the incorporation of Ru atoms into the Pt lattice [11] suggesting the formation of Pt-Ru alloy or solid solutions [12]. As discussed above, PtRu blacks are bulk mixtures of Pt metal, Pt hydrous oxides and hydrous and dehydrated RuO_2. In fact, Ru metal accounts to only a minor fraction (<25%) of the total ruthenium species [6].

3.1.2. TPR

Prior to the TPR analysis, samples were dried for 1 h at 100 °C under He flow and cooled in a water at ca. 4 °C in order to avoid undesired reactions when the H_2/Ar flow is passed through the sample [13]. TPR profiles of Ru-fresh, Ru-calcined, PtRu-fresh and PtRu-He are depicted in Fig. 3. In good agreement with XRD analysis, samples Ru-fresh and Ru-calcined display distinct TPR profiles. Hydrogen consumption on sample Ru-fresh occurs at much lower temperatures around ca. 90 °C whereas the maximum hydrogen consumption on Ru-calcined is centered at 158 °C. This latter process has been assigned to the reduction of RuO_2 [14]. Both XRD and TPR analysis coincide in that different Ru species are stabilized on each of those samples, RuO_2 being the most abundant in Ru-calcined. On the other hand, since the reduction of Ru-fresh occurs at lower temperatures it is reasonable to assume that a less oxidized Ru phase is the main one in this sample. Furthermore, this sample is an amorphous Ru species as deduced from XRD. The narrow hydrogen consumption peak at 90 °C in Ru-fresh is assigned to the reduction of amorphous ruthenium oxide [14].

The TPR profiles of the Pt-containing samples are broader and more complicated. When Pt its introducing in the synthetic procedure modifies the conditions of preparation such as pH or chloride concentration [15]. PtRu-fresh shows two reduction processes centered at 98 and 173 °C. By comparison with the TPR of the reference bare Ru samples these peaks could be assigned to the reduction of oxide phases akin to those present in Ru-fresh and Ru-calcined samples, *i.e.* amorphous Ru oxide and crystalline RuO_2, respectively. Attention should be paid to the fact that peaks are quite broad, which is indicative that several oxides types might

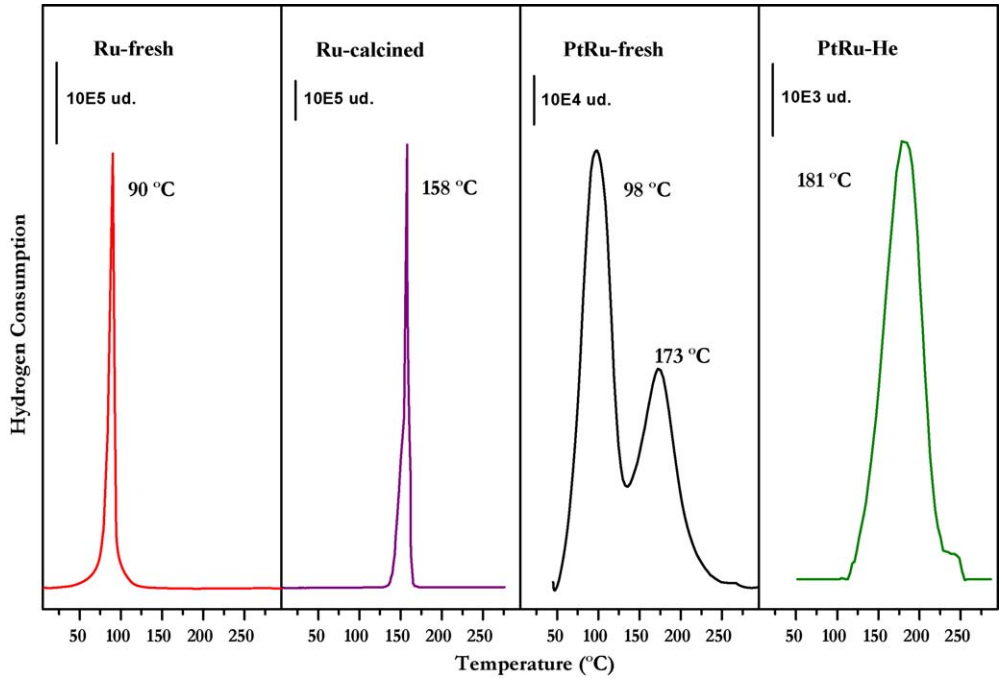

Fig. 3. Hydrogen consumption profile (TPR) of Ru-fresh, Ru-calcined, PtRu-fresh and PtRu-He.

Table 1
Data XPS spectra of Ru alone samples.

Sample	BE Ru 3d (eV)	FWMH	Ru species	BE O 1s (eV)	FWMH	O/Ru
Ru-reduced	280.1 (67)	1.55	Ru^0	529.9 (45)	2.05	
	281.3 (21)	1.55	RuO_2 anh.	531.7 (41)	2.05	0.98
	282.6 (12)	1.45	$RuO_2{\cdot}xH_2O$	533.0 (13)	1.99	
Ru-calcined	281.6 (68)	2.2	RuO_2 anh.	529.8 (42)	2.03	
	283.5 (32)	2.3	$RuO_x(OH)_y$	531.3 (44)	2.05	3.27
				533.0 (14)	2.05	
Ru-fresh	282.3 (69)	2.15	$RuO_2{\cdot}xH_2O$	530.0 (51)	2.05	
	284.1 (31)	2.15	$RuO_x(OH)_y$	531.4 (32)	2.04	3.87
				533.1 (17)	2.05	

coexist in the solid. However, the TPR profile of sample PtRu-He displays a single broad reduction peak centered at 181 °C. This indicates that after thermal treatment RuO_2 remains as the only oxidized species in the sample.

It has been reported that platinum could be reduced at lower temperatures (−3 °C) [16]. The TPR device employed in this work does not allow low temperature analysis therefore the presence of Pt-rich islands on the catalysts surface cannot be ruled out.

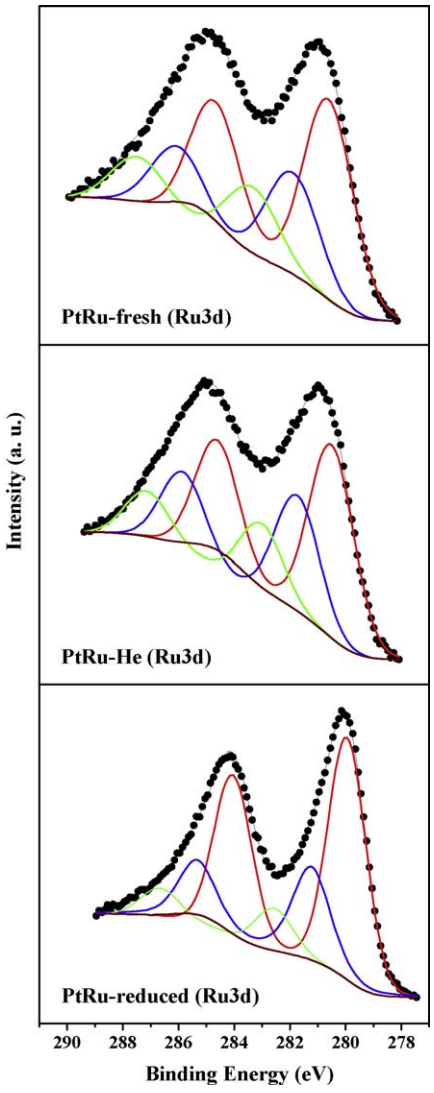

Fig. 4. XPS spectra of Ru 3d core-level PtRu-fresh, PtRu-He, and PtRu-reduced.

3.1.3. XPS analysis

To determine the oxidation states on the samples, XPS analyses of C 1s + Ru 3d, Pt 4f and O 1s core-level regions were carried out. Table 1 summarizes binding energies (BE), relative intensity (%) and O/Ru ratio derived from the XPS analyses. Ru 3d core-level spectra are shown in Fig. 4. The Ru 3d core-level region on XPS spectrum coincides with that of the C 1s. However, since bulk PtRu instead of carbon supported PtRu have been prepared, our XPS analysis is adequate enough to discriminate ruthenium contribution from any carbon contamination.

For setting the adequate references for XPS analysis, samples RuAu, either reduced or fresh, were used as reference by setting the Au $4f_{7/2}$ core-level at 84.0 eV as explained above. In sample RuAu-reduced three Ru species at 280.1, 281.3 and 282.6 eV were detected. According to literature they were assigned to Ru^0, RuO_2 and $RuO_2{\cdot}xH_2O$, respectively. For the RuAu-fresh sample, the Ru $3d_{5/2}$ core-level was deconvoluted into two species at 281.7 and 283.7 eV assigned, respectively to RuO_2 and to amorphous Ru oxide (its actual nature will be discussed below) [4].

For the assignment of the XPS peaks several options exists. For instance, binding energies of 282.6 and 283.5 eV have been assigned to RuO_3 (Ru^{VI}) or RuO_4 (Ru^{VIII}) [17,18]. However, in this work, the presence of either RuO_3 or RuO_4 phase is put aside in favor of hydrous ruthenium dioxide [7]. RuO_3 has not been reported as a solid phase being stable only as a vapor phase from 1200 to 1500 °C. RuO_4 is formed at temperatures above 250 °C, decomposing upon cooling to form RuO_2 [19,20].

By comparing the Ru 3d spectra of the RuAu it appears that two types of ruthenium oxides might be stabilized: (i) ruthenium dioxide anhydrous (RuO_2) displaying a rutile like structure at ca. 281.3 eV; (ii) a broad peak that contains a number of hydrous Ru oxides. Whereas RuO_2 is a crystalline phase, the hydrous ones are amorphous. There are also important differences in the reduction pattern of each species. The crystalline ones display a hydrogen consumption peak at ca. 158 °C and the amorphous phase is reduced at lower temperatures of ca. 90 °C as discussed above. It must be taken into account that the ruthenium oxide phase corresponds to a non-stoichiometric form comprising a number of oxoruthenium states involving all three oxygen-containing species, and with water as the source of both the oxygen and hydroxyl groups [7]. In fact, it is well established that Ru and RuO_2 chemisorb oxygen and water strongly [5,21]. It is generally accepted that hydrous ruthenium oxide species appears at binding energies of 1–2 eV higher than RuO_2 in the form of a rather broad peak (FHMW > 5 eV) in the XPS spectrum [22]. In the XPS analysis undertaken in here, we have gone further and we have considered the presence of two main components: (a) hydrous ruthenium dioxide ($RuO_2{\cdot}xH_2O$) with a variable amount of surface chemisorbed water at 282.6 eV; and (b) $RuO_x(OH)_y$ at higher binding energies ca. 283.7 eV. For this case, FHMW of around 2.0 eV were used.

Table 2
Binding energy, FWMH and assignment of the species from the XPS.

Sample	BE Ru $3d_{5/2}$ (eV)	FWHM	Ru species	BE Pt $4f_{7/2}$ (eV)	FWHM	BE O 1s (eV)	FWHM	Pt/Ru	O/M
PtRu-reduced	280.0 (62)	1.6	Ru^0	71.5 (65)	2.05	529.9 (56)	2	1.17	0.78
	281.2 (27)	1.6	RuO_2 anh.	73.6 (27)	2.05	531.4 (31)	1.89		
	282 6 (11)	1.6	$RuO_2{\cdot}xH_2O$	75.5 (8)	2.15	533.0 (13)	2.06		
PtRu-He	280.5 (53)	1.9	Ru^0	71.4 (62)	2.15	529.7 (60)	1.9	0.64	1.50
	281.7 (28)	1.81	RuO_2 anh.	73.5 (29)	2.19	531.3 (31)	1.9		
	283.0 (19)	1.85	$RuO_x(OH)_y$	75.6 (9)	2.2	533.1 (8)	1.94		
PtRu-fresh	280.6 (53)	2.05	Ru^0	71.5 (64)	2.17	530.0 (69)	2.16	0.97	1.29
	281.9 (28)	2.05	RuO_2 anh.	73.6 (28)	2.17	531.7 (24)	2.15		
	283.4 (19)	2.05	$RuO_x(OH)_y$	75.6 (8)	2.22	533.2 (7)	2.15		
Pt-reduced	–	–	–	70.3 (63)	2.05	529.7 (36)	2.02	–	2.89
				72.3 (27)	2.15	531.3 (40)	2.05		
				74.3 (10)	2.15	532.8 (23)	2.05		

M = Pt + Ru.

The Ru 3d $_{5/2}$ core-level spectrum of Ru-calcined contains two contributions at 281.6 and 283.5 eV. In line with peak assignment described above these peaks are ascribed to RuO_2 and $RuO_x(OH)_y$. XRD and TPR analysis of the Ru-calcined sample only reveal the presence of RuO_2 but it is not unlikely that surface hydration has taken place. The XPS spectrum of Ru-fresh displays the $Ru3d_{5/2}$ components at 282.3 and 284.1 eV, assigned to $RuO_2{\cdot}xH_2O$ and $RuO_x(OH)_y$, respectively. The Ru 3d $_{5/2}$ core-level spectrum of Ru-reduced contains three contributions at 280.1, 281.3 and 282.6 eV assigned to Ru^0, RuO_2 and $RuO_2{\cdot}xH_2O$, respectively. In order to further corroborate the goodness of the XPS analysis special attention was paid to the O 1s core-level region. It is generally accepted that the binding energy of the O 1s core-level for noble- and transition metal oxides is centered at ca. 530.0 eV. Hydroxides and adsorbed water appear at 532.0 and 533.0 eV, respectively [8].

With respect to the nature of surface species on Pt and PtRu samples, Table 2 depicts the binding energy, relative intensity (%), Pt/Ru ratio and O/(Pt + Ru) of the Pt4f, Ru3d and O 1s core-levels of all catalysts. The XPS spectra of Pt-reduced reveals the presence of Pt^0, Pt^{II} and Pt^{IV} at 70.3, 72.3 and 74.3 eV. In the bimetallic catalysts the most abundant Pt species is Pt^0 which in the XPS spectra appears at 71.4 eV. This shifting, as compared to bare-Pt is related to alloying effects or a Pt-rich surface [23]. The O 1s core-level of the XPS spectra of Pt and PtRu display three components at the binding energies expected for metal oxide, hydroxide and adsorbed water. Results are given in Table 2. The XPS analysis of the Ru 3d core-level region of PtRu-reduced reveals three species at 280.0, 281.2 and 282.6 eV. In line with the XPS reference spectra described above these species were assigned as Ru^0, RuO_2 and $RuO_2{\cdot}xH_2O$, respectively.

PtRu-fresh comprises three Ru species as 280.6, 281.9 and 283.4 eV. The same applies to PtRu-He with species at 280.5, 281.7 and 283.0 eV. In both samples the peak at lower binding energy was assigned as Ru^0. However, a shifting to higher binding energies is observed. The magnitude of the shifting was adjusted by the O 1s core-level region. The peaks at 281.9 or 281.7 eV correspond to anhydrous RuO_2. The peaks at higher binding energies are assigned to $RuO_x(OH)_y$.

3.2. Electrochemical characterization

3.2.1. CO stripping

Surface area of Pt was estimated by CO stripping analysis assuming that for high CO coverage linear bound CO is the dominant state on platinum surfaces [24]. The amount of adsorbed CO was evaluated by integration of the CO stripping peak, corrected for the electric double-layer capacitance. Thus, the charge for the oxidation of fully CO-covered surface can be taken as 420 $\mu C/cm^2$ [25]. Table 3 summarizes the electrocatalytically active area (EAA), the onset potentials for CO oxidation (E_{onset}) and peak potentials (E_p) on PtRu and Pt, as well the average crystal size deduced by the Scherrer equation and surface area (S), calculated from the XRD reflection 220 in Pt-content catalyst. EAA value follows the trend: PtRu-fresh > PtRu-He > PtRu-reduced > Pt-reduced. Among other features, the value of the EAA relates to

Table 3
Electrochemical parameters deduced from the CO stripping analysis. Crystal size and surface area (S), calculated from XRD.

Sample	E_{onset} (V vs. NHE)	E_p (V vs. NHE)	EAA (m^2/g)	Particle size (nm)	S (m/g)
PtRu-reduced	0.38	0.50	28.76	7.1	39.5
PtRu-fresh	0.39	0.51	73.76	7.9	35.5
PtRu-He	0.39	0.52	56.57	8.1	34.6
Pt-reduced	0.39	0.67	14.55	11.4	24.6

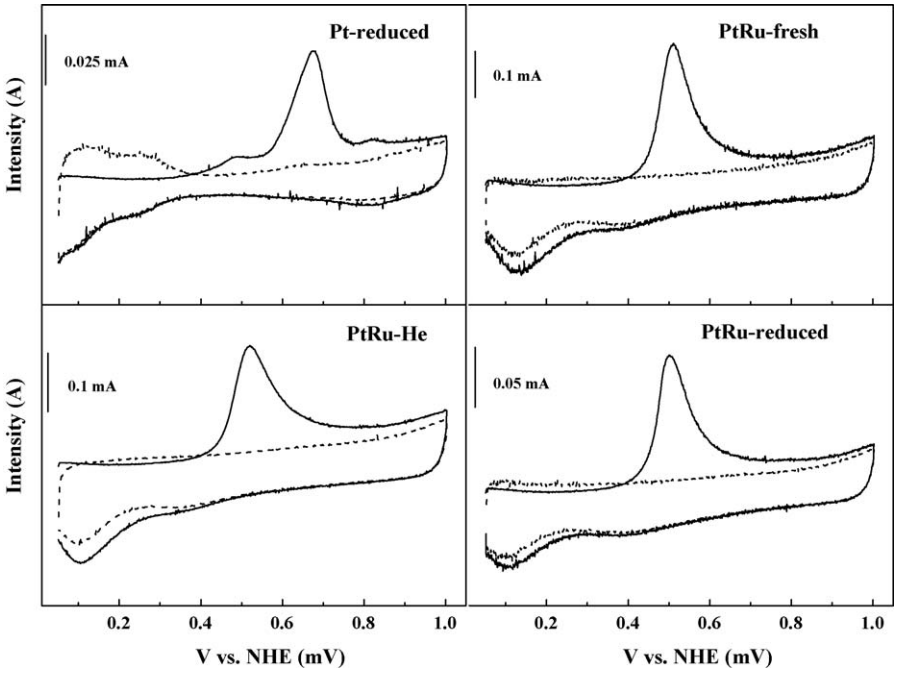

Fig. 5. CO stripping analysis of Pt-reduced, PtRu-fresh, PtRu-He and PtRu-reduced samples (black line). The voltammogram recorded after the stripping analysis is depicted in dot line.

the average particle size and, consequently, to the amount of exposed Pt, displaying larger particles sizes either PtRu samples under thermally treatment of Pt [26].

Fig. 5 depicts base voltammograms (dashed line) and CO oxidation (solid line) on PtRu and Pt samples recorded at 10 mV/s in 0.5 M $HClO_4$. In the presence of CO the hydrogen adsorption–desorption features are not observed. After CO oxidation (reverse scan) the hydrogen features can be observed. The CO oxidation pattern is similar in all PtRu electrocatalysts regardless of thermal treatment. The onset of the process occurs at ca. 380 mV. The CO oxidation pattern on Pt displays two processes, the main one starting at ca. 580 mV with E_p at 820 mV in good agreement with previously reported results [27]. Recent NMR studies reveal two types of CO_{ads} species, with no rapid exchange between the two populations [25] responsible of both oxidation processes. The shifting of the CO oxidation process on PtRu accounts to its facility in nucleating OH_{ad} species at less positive potential than Pt. According to the bifunctional model, oxophilic Ru sites covered by –OH would play a key role as the oxygen source to oxidize CO, being the actual source of oxygen required for surface CO removal at low potentials [28].

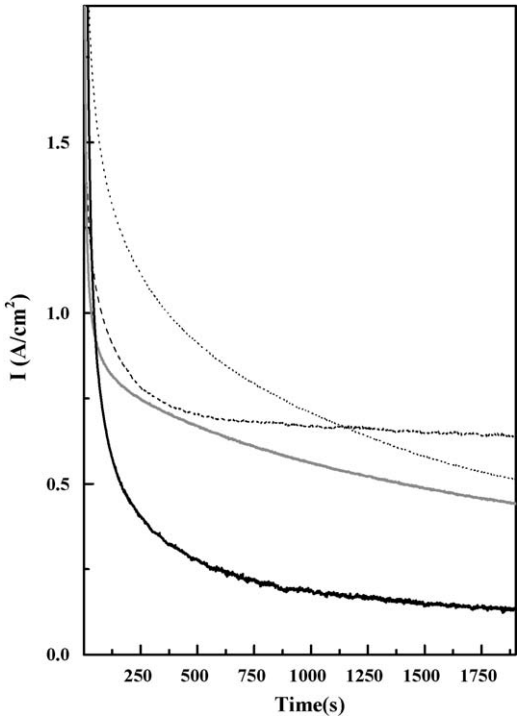

Fig. 6. Chronoamperometry in 0.5 M H_2SO_4 + 2 M CH_3OH of samples Pt-reduced (black), PtRu-He (grey), PtRu-fresh (dash) and PtRu-reduced (dot).

3.2.2. Methanol oxidation

The reactivity of PtRu and Pt samples towards methanol oxidation was tested by chronoamperometry. The current densities depicted in Fig. 6 are normalized to the EAA obtained from CO stripping. PtRu catalysts display more active sites for methanol oxidation than Pt. In fact, during the early stages of the reaction PtRu-reduced is the most active sample. During reaction both PtRu-reduced and PtRu-He lose their activity, this sample suffers a severe deactivation process, especially PtRu-reduced one. On the contrary sample PtRu-fresh is quite stable during the experiment. As expected, Pt is the less active sample in the methanol oxidation reaction under the studied conditions than PtRu with a stoichiometry close to 1:1 [29]. PtRu-reduced displays the largest Pt/Ru surface ratio and the largest amount of surface Pt^0 as deduced from the XPS analysis (see Table 2). This feature could explain both the highest activity of this sample during the early stages of the reaction and its rapid deactivation. On the one side, Pt is more active than Ru in oxidizing methanol (hence the highest activity) but on the other hand it becomes rapidly deactivated as soon as CO species are formed.

As to why PtRu-fresh is the most stable sample under reaction conditions we can hypothesize on two parallel lines. First, it has a

Pt/Ru stoichiometry close to 1, which is reported as the most adequate for methanol oxidation. Besides, it has the largest amount of hydrous RuO_2, especially in the form of $RuO_x(OH)_y$ which are the most active phases for enhancing the tolerance to CO [4,6].

4. Conclusions

The chemical state of Ru in PtRu samples comprises a series of anhydrous and hydrous Ru oxide phases. While anhydrous RuO_2 is a crystalline phase, the hydrous phases are amorphous. From the XPS analysis, we have identified two hydrous ruthenium oxide phases: $RuO_2{\cdot}xH_2O$ and $RuO_x(OH)_y$, displaying different binding energies. The actual role of each phase is unclear although both are amorphous phases that seem to improve the durability of the catalysts during the methanol electrooxidation reaction as compared to the samples where crystalline RuO_2 is the predominant Ru oxide phase. The samples containing metallic phases of Pt and Ru are the most active in the methanol electrooxidation reaction although they show a rapid deactivation.

References

[1] A.S. Aricó, S. Srinivasan, V. Antonucci, Fuel Cells 1 (2001) 133.
[2] T. Frelink, W. Vissher, J.A.R. van Veen, Surf. Sci. 335 (1995) 353.
[3] B. Yang, Q. Lu, Y. Wang, L. Zhuang, J. Lu, P. Liu, Chem. Mater. 15 (2003) 3552.
[4] D.R. Rolison, P.L. Hagan, K.E. Swider, J.W. Long, Langmuir 15 (1999) 774.
[5] A.S. Aricó, G. Monforte, E. Modica, P.L. Antonucci, V. Antonucci, Electrochem. Commun. 2 (2000) 466.
[6] J.W. Long, R.M. Stroud, K.E. Swider-Lyons, D.R. Rolison, J. Phys. Chem. B 104 (2000) 9772.
[7] J.M. Fletcher, W.E. Gardner, B.F. Greenfield, M.J. Holdoway, M.H. Rand, J. Chem. Soc. A (1968) 653.
[8] M. Vukovik, T. Valla, M. Milun, J. Electroanal. Chem. 356 (1993) 81.
[9] T.L. Stuchinskaya, M. Musawir, E.F. Kozhevnikova, I.V. Koxhevnikov, J. Catal. 231 (2005) 41.
[10] W. Kraus, G. Nolze, J. Appl. Cryst. 29 (1996) 301.
[11] A.S. Arico, P.L. Antonucci, E. Modica, V. Baglio, H. Kim, V. Antonucci, Electrochim. Acta 47 (2002) 3723.
[12] E. Antolini, L. Giorgi, F. Cardellini, E. Passalacqua, J. Solid State Electrochem. 5 (2001) 131.
[13] D. Chu, S. Gilman, J. Electrochem. Soc. 143 (1996) 1685.
[14] S.-Y. Huang, S.-M. Chan, C.-T. Yeh, J. Phys. Chem. B 110 (2006) 234.
[15] J.A. Rard, Chem. Rev. 85 (1985) 1.
[16] T. Mahmood, J.O. Williams, R. Miles, B.D. McNicol, J. Catal. 72 (1981) 218.
[17] W. Eberhardt, P. Fayet, D.M. Cox, Z. Fu, A. Kaldor, R. Sherwood, D. Sonddericker, Phys. Rev. Lett. 64 (1990) 780.
[18] R. Liu, H. Iddir, Q. Fan, G. Hou, A. Bo, K.L. Ley, E.S. Smotkin, Y.-E. Sung, H. Kim, S. Thomas, A. Wieckowski, J. Phys. Chem. B 104 (2000) 3518.
[19] A.S. Arico, V. Baglio, A. Di Blasi, E. Modica, P.L. Antonucci, V. Antonucci, J. Electroanal. Chem. 557 (2003) 167.
[20] P. Froment, M.J. Genet, M. Devillers, J. Electron Spectr. Relat. Phenom. 104 (1999) 119.
[21] H. Yeung, H. Chan, C.G. Takoudis, M.J. Weaver, J. Catal. 172 (1997) 336.
[22] R.K. Raman, A.K. Shukla, A. Gayen, H.S. Hedge, K.R. Priolkar, P.R. Sarode, S. Emura, J. Power Sources 157 (2006) 45.
[23] A.K. Shukla, A.S. Arico, K.M. El-Khatib, H. Kim, P.L. Antonucci, V. Antonucci, Appl. Surf. Sci. 137 (1999) 20.
[24] T.J. Schmidt, M. Noeske, H.A. Gasteiger, R.J. Behm, P. Britz, H. Bönnemann, J. Electrochem. Soc. 145 (1998) 925.
[25] S.A.M. Silva, J. Pérez, R.M. Torresi, C.A. Luengo, E. Ticianelli, Electrochim. Acta 44 (1999) 3565.
[26] A. Pozio, M. De Francesco, A. Cemmi, F. Cardellini, L. Giorgi, J. Power Sources 105 (2002) 13.
[27] S. Ball, A. Hodgkinson, G. Hoogers, S. Maniguet, D. Thompsett, B. Wong, Electrochem. Solid State Lett. 5 (2002) A31.
[28] T. Iwasita, H. Hoster, A. John-Anacker, W.F. Lin, W. Vielstich, Langmuir 16 (2000) 522.
[29] H.A. Gasteiger, N. Markovic, P.N. Ross Jr., E.J. Carns, Electrochim. Acta 39 (1994) 1825.